Sustainable Materials and Technologies 29 (2021) e00294

Contents lists available at ScienceDirect

Sustainable Materials and Technologies

journal homepage: www.elsevier.com/locate/susmat

Density functional theory study on the enhanced adsorption mechanism of gaseous pollutants on Al-doped Ti_2CO_2 monolayer

Zechao Wu [a,b], Junhui Zhou [a], Didi Li [a], Zhimin Ao [a,*], Taicheng An [a], Guoxiu Wang [c]

[a] Guangzhou Key Laboratory Environmental Catalysis and Pollution Control, Guangdong Key Laboratory of Environmental Catalysis and Health Risk Control, School of Environmental Science and Engineering, Institute of Environmental Health and Pollution Control, Guangdong University of Technology, Guangzhou 510006, China
[b] School of Materials Science and Engineering, Dongguan University of Technology, Dongguan 523808, China
[c] Centre for Clean Energy Technology, University of Technology Sydney, 15 Broadway, Sydney, New South Wales 2007, Australia

ARTICLE INFO

Article history:
Received 5 March 2021
Received in revised form 12 May 2021
Accepted 16 May 2021

Keywords:
Gaseous pollutants
Adsorbent
MXene
Al doping
DFT calculations

ABSTRACT

Inorganic toxic gases (ITGs) and volatile organic compounds (VOCs) are two kinds of typical hazardous gaseous pollutants harming human health. The removal of them is still an enormous challenge. Based on density functional theory (DFT) calculations in this work, Al-doped Ti_2CO_2 (ATCO), a single-atom-decorated MXene, is expected to be a more effective adsorbent for these gases than pristine Ti_2CO_2 (TCO) due to the outstanding adsorption capacity and superb electrical properties. We then shed light on the mechanism of enhanced adsorption by ATCO. The results of Mulliken charge analysis, partial density of states (PDOS) and deformation charge density (DCD) confirm the change of charge distribution on ATCO surface after the decoration of Al atom. Obviously, Al atom can act as a bridge to promote the formation of chemical bonds between the adsorbed gases and ATCO substrate. This work not only provides a promising material for the adsorption of gaseous pollutants, but also explores a new avenue for designing and fabricating MXene-based non-noble metal materials in the area of gas adsorbents.

1. Introduction

Nowadays, human beings are confronted with many environmental problems, among which air pollution is one of the most severe challenges worldwide. Generally speaking, gaseous pollutants in the atmosphere are comprised of two kinds of gases, including primary pollutants and secondary pollutants [1,2]. The former mainly contains CO, SO_2, NO, NH_3, H_2S and hydrocarbons, and the latter contains O_3, NO_2, SO_3, aldehydes and ketones, *etc.* From another perspective, gaseous pollutants can also be divided into two categories: inorganic toxic gases (ITGs) and volatile organic compounds (VOCs). The majority of gaseous pollutants have pungent smell and toxicity, and may cause allergies, dyspnea, asthma and even cancers, especially when human body is exposed to the high concentration surroundings of these gases for a long time [3,4]. In order to control the emission of gaseous pollutants, a series of techniques have been taken, including adsorption [5,6], catalytic oxidation [7,8], photocatalysis [9,10] and biological degradation [11]. In the midst of these methods, adsorption has been proved to be the most common and effective method to remove gaseous pollutants, while the efficiency of adsorbents is affected by many factors, such as selectivity, specific surface area and convenience of maintenance [12,13].

Currently, researches of MXenes, a class of emerging two-dimensional (2D) transition metal carbides or carbonitrides, have boosted rapidly since the first kind of MXene—Ti_3C_2 was synthesized in 2011 [14–16]. It is worthy to note that MXenes ($M_{n+1}X_nT_x$) can be synthesized by etching from MAX ($M_{n+1}AX_n$) phases [17], where "M" denotes early *d*-orbital transition metals, $n = 1, 2$, or 3, "X" represents C and/or N, "T" refers to functionalized terminations (–F, –O and –OH), "x" stands for the number of termination groups, and "A" mainly composes of the elements of the group III A and IV A [14,16]. The bare MXenes without T_x terminations, for example, Ti_2C and Ti_3C_2, show metallic characteristics, whereas they were found to be unstable [18,19]. As for functionalized MXenes, their terminations are determined by the specific experimental conditions, including etchant selection and the subsequent treatment process [20,21]. For instance, –F groups on MXenes would be displaced by -OH groups when they are stored in water [16], while -OH functionalized MXenes could turn into –O functionalized one at high temperature [22]. Inevitably the terminal groups can make remarkable influence to the performance of MXenes [23].

Although great progress has been made in the researches of MXenes in the last decade, the application of MXenes is mainly at a nascent stage at present compared with graphene and other 2D materials. There is still a long way before large-scale industrial application [24]. Nevertheless, MXenes have been still regarded as a sort of promising materials because of their excellent electrical conductivity, formidable chemical and mechanical stability, abundant active sites and large

---

* Corresponding author.
E-mail address: zhimin.ao@gdut.edu.cn (Z. Ao).

https://doi.org/10.1016/j.susmat.2021.e00294
2214-9937/© 2021 Elsevier B.V. All rights reserved.

specific surface area [25–27]. In fact, MXenes are expected to be applied in expansive fields such as photo/electrocatalysis [28–31], energy storage [22,32,33], gas sensors [34–37] and electromagnetic absorption/shielding [38] in the future.

Among dozens of MXenes, M_2CT_2 (M = Ti, Zr, Hf and Sc) have attracted intensive attention at theoretical level by their unique natures, while many research groups have predicted the structures, band gaps and optical properties of them [28,29,39–42]. It is reported that M_2CT_2 possess outstanding stability when their terminations are composed of –O groups, since the cohesive energies of M_2CO_2 are more negative than those of M_2CF_2 or $M_2C(OH)_2$ [41,43]. In addition, the –O terminations would be able to protect the internal metal atoms of MXenes from being exposed to the environment, hence maintaining the stability of MXenes [44]. In the utilization of M_2CO_2 as gas sensors, Xiao et al. made a pioneering research. They predicted that Ti_2CO_2 and Zr_2CO_2 can detect NH_3 with high sensitivity and selectivity [34,35]. More recently, Junkaew et al. and Jiao et al. respectively studied the adsorption of a series of inorganic gases on MXenes, and they also discovered that Ti_2CO_2 [45] and Hf_2CO_2 [46] were potential for NH_3 detection and storage.

Single-atom catalysts (SACs), contrived by Zhang et al. in 2011 [47], have been one of the research hotspots and cutting-edge domains in the area of catalysis. SACs can remarkably increase the efficiency of atomic utilization owing to the size reduction, while they have significantly lower cost and higher selectivity than undecorated catalysts [48]. Owing to its elaborate activated reaction site, single-atom-decorated MXenes have manifested more prominent performance than pristine MXenes in hydrogen evolution reaction (HER) [30,49], oxygen reduction reaction (ORR) [44], CO oxidation [7,50,51] and nitrogen reduction reaction (NRR) [52,53]. According to the previous studies of our research group, the Al-doped C_2N [12,54], Al-doped graphene [55,56] and Al-doped porous graphene [6] have been proven to bring about a vast improvement in the adsorption of ITGs and VOCs, while Ti-decorated $Ti_3C_2O_2$ and V-decorated Ti_2CO_2 has been turned out to be a promising non-noble metal catalytic system for HCHO oxidation [57] and H_2S decomposition [58], respectively.

Inspired by previous studies, three structure-like M_2CO_2 (Ti_2CO_2, Zr_2CO_2 and Hf_2CO_2) are chosen as the adsorbents to remove gaseous pollutants, and single-atom-decorated method is taken to enhance the capability of adsorbents in this work. DFT calculations are carried out to acquire comprehensive cognition on the adsorption mechanisms of ITGs and VOCs on the M_2CO_2 and single-atom-decorated M_2CO_2. It is expected that our work will provide a conceivable 2D material and illuminate theoretical guidance for constructing efficient nano-catalysts for gaseous pollutants adsorption.

2. Computational framework

DFT calculations with the spin unrestricted approach are implemented in DMol3 module of Materials Studio software [59]. The generalized gradient approximation (GGA) method with Perdew-Burke-Ernzerhof (PBE) functional is adopted to describe the exchange correlation function [60]. Considering the van der Waals forces between the MXenes and gas molecules, the Grimme method for DFT-D correction is used for all calculations [61]. Double numerical plus polarization (DNP) is adopted as the basis set to expand the molecular orbitals, and DFT Semi-core Pseudopotentials (DSPP) is employed to dispose of the nuclear electrons [62]. The convergence tolerance of energy is 1.0×10^{-6} Ha/atom, while the maximum permissible displacement and force are 0.005 Å and 0.002 Ha/Å, respectively. The smearing value is set as 0.005 Ha, and the Brillouin zone is indicated by a Monkhorst-Pack $4 \times 4 \times 1$ k-point mesh. In order to avoid the interlayer interaction, a vacuum layer of about 15 Å is established along the z-axis, while all the atoms of the system are allowed to relax. The electronic density distribution and the Mulliken charge analysis method is utilized to calculate the charge transfers. Additionally, molecular dynamics (MD) simulations are adopted to evaluate the thermal stability. MD simulation in a NVT ensemble continues for 5 ps with a time step of 2.0 f. [7], and the Nosé-Hoover method is used to control temperature of the system [63].

Based on the characteristics of the M_2CO_2 unit cells, $3 \times 3 \times 1$ hexagonal supercell are built. The binding energy is defined as follows:

$$E_b = E_{MXene+atom} - E_{MXene} - E_{atom} \quad (1)$$

where $E_{MXene+atom}$, E_{MXene} and E_{atom} denote the energies of MXene with single-atom decoration, MXene monolayer and the doped atom, respectively.

When one gas molecule is adsorbed on MXene, the adsorption energy is defined as follows:

$$E_{ad} = E_{MXene+gas} - E_{MXene} - E_{gas} \quad (2)$$

where $E_{MXene+gas}$, E_{MXene} and E_{gas} denote the energies of MXene with gas adsorption, MXene monolayer and gas molecule, respectively.

3. Results and discussion

3.1. Geometry optimization and electronic properties of MXenes

3.1.1. Geometry optimization of M_2CO_2 and single-atom-decorated M_2CO_2

According to previous work, Ti_2CO_2, Zr_2CO_2 and Hf_2CO_2 have four types of structures [29,39,41]. The most stable structures of them are similar and Fig. 1(a) shows the most stable configuration of Ti_2CO_2 as an example. The configuration has three typical decorating sites for the doping of single atoms. On site *a*, the doped atom is located at the hollow site between three adjacent O atoms and right above the C atom; on site *b*, the doped atom is set right above the O atom; and on site *c*, the doped

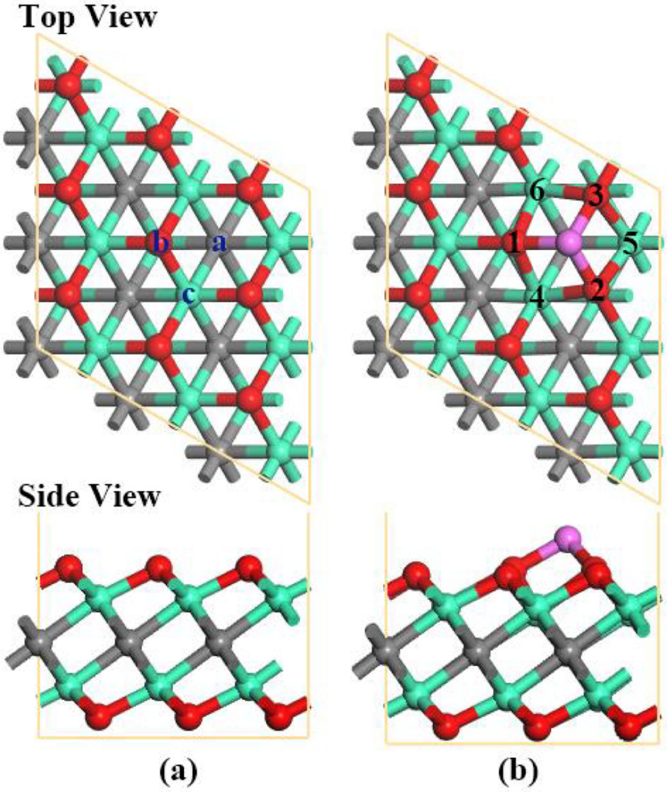

Fig. 1. (a) The most stable structure of pristine Ti_2CO_2 after optimization. The most stable structure of Zr_2CO_2 and Hf_2CO_2 is similar and thus is omitted. The letters in this figure represent the possible decorating sites. (b) The most stable structure of Al-doped Ti_2CO_2 after optimization. The most stable structure of B-doped Ti_2CO_2 is similar and thus is omitted. The numbers in this figure represent the order of O and Ti atoms. The grey, red, pink and cyan balls in this and the following figures are C, O, Al and Ti atoms, respectively.

atom is right above the M atom [7]. After geometry optimization, the lattice parameters of Ti_2CO_2, Zr_2CO_2 and Hf_2CO_2 are relaxed to $a = b = 9.207$ Å, $a = b = 9.981$ Å and $a = b = 9.429$ Å, respectively.

To investigate the stability of doped atoms on the M_2CO_2 surface, we choose seven non-noble metal free elements from the group III A to the group VI A (B, C, N, Al, Si, P and S), which are common and low-cost in experiment. According to Table S1 and Fig. 2(a), the calculated binding energy of B and Al atom at the site *a* of Ti_2CO_2 is −6.25 eV and − 3.77 eV respectively, which is more negative than their corresponding cohesive energy (−5.81 eV and −3.39 eV respectively). The result indicates that these two atoms can be easily dispersed on Ti_2CO_2 (TCO) substrate without the formation of clusters. However, such situation does not occur in the decoration of all the other elements on TCO and all the seven elements on Zr_2CO_2 and Hf_2CO_2. More importantly, aggregation of doped atoms should be avoided for the reason that gas adsorption capacity of 2D materials may be weakened [55]. Therefore, only B-decorated Ti_2CO_2 (BTCO) and Al-decorated Ti_2CO_2 (ATCO) are considered in the following calculations, and the most stable structure of them is displayed in Fig. 1(b).

3.1.2. Electronic properties of TCO, BTCO and ATCO

To explore the electronic properties of TCO, BTCO and ATCO, we calculate the Mulliken charge distributions, the partial density of states (PDOS) and the deformation charge density (DCD) of them. According to Table S1, 0.365 e charge transfers from B atom to TCO surface, whereas 1.245 e charges transfer from Al atom to TCO. Subsequently, six ambient atoms including three O atoms and three Ti atoms around the doped site *a* are chosen to assess the charge transfer situation, as shown in Fig. 1(b). As for Table S2, it shows that not only the charges of individual O and Ti atom around the Al atom but also the total atomic charges of these six atoms are more negative than those of B atom and those on TCO surface. Obviously, Al atom provides more electrons for neighboring atoms than B atom, indicating that ATCO is able to bring stronger interaction between the Al atom and the TCO substrate than that of B atom and the TCO substrate in BTCO.

As represented in Fig. 2(b) and (c), the PDOS of TCO near the Fermi level is mostly contributed by the 3*d*-orbital of Ti atoms [19], while that of BTCO is similar with TCO. As for ATCO, there is high hybridization between 2*p*-orbital of O atoms, 3*p*-orbital of Al atom and 3*d*-orbital of Ti atoms near the Fermi level (Fig. 2(d)), which is more powerful than those of TCO and BTCO. It is also easy to discover that BTCO has a strong hybridization between the 2*p*-orbital of the B atom and the 2*p*-orbital of O atom at about −7.5 eV below the Fermi level, while there is also a forceful hybridization of ATCO between the 3*p*-orbital of the Al atom and the 2*p*-orbital of O atom at about −6 eV below the Fermi level.

Meanwhile, the DCD of BTCO and ATCO is analyzed and illustrated in Fig. 3(a) and (b), where the red and blue areas represent electron gain and loss respectively. It is easy to observe that electrons are transferred from B and Al atom to their neighboring three O atoms so that they can establish chemical bonds with these O atoms, and the bond length of Al–O (1.822 Å) is longer than that of B–O (1.405 Å), which is in good agreement with the results of Mulliken charge analysis shown in Table S1 and Table S2. As a consequence, ATCO is supposed to possess a stronger adsorption capacity for ITGs and VOCs molecules than TCO and BTCO, owing to the more positively charged Al dopant and more negatively charged TCO substrate, which can play a vital role in the adsorption of these molecules. Therefore, BTCO is no longer considered in the next part of this work.

3.1.3. Stability of ATCO

The thermal stability of ATCO is assessed by MD simulations. As shown in Fig. 4(a–c), the configuration of ATCO is well retained at 300

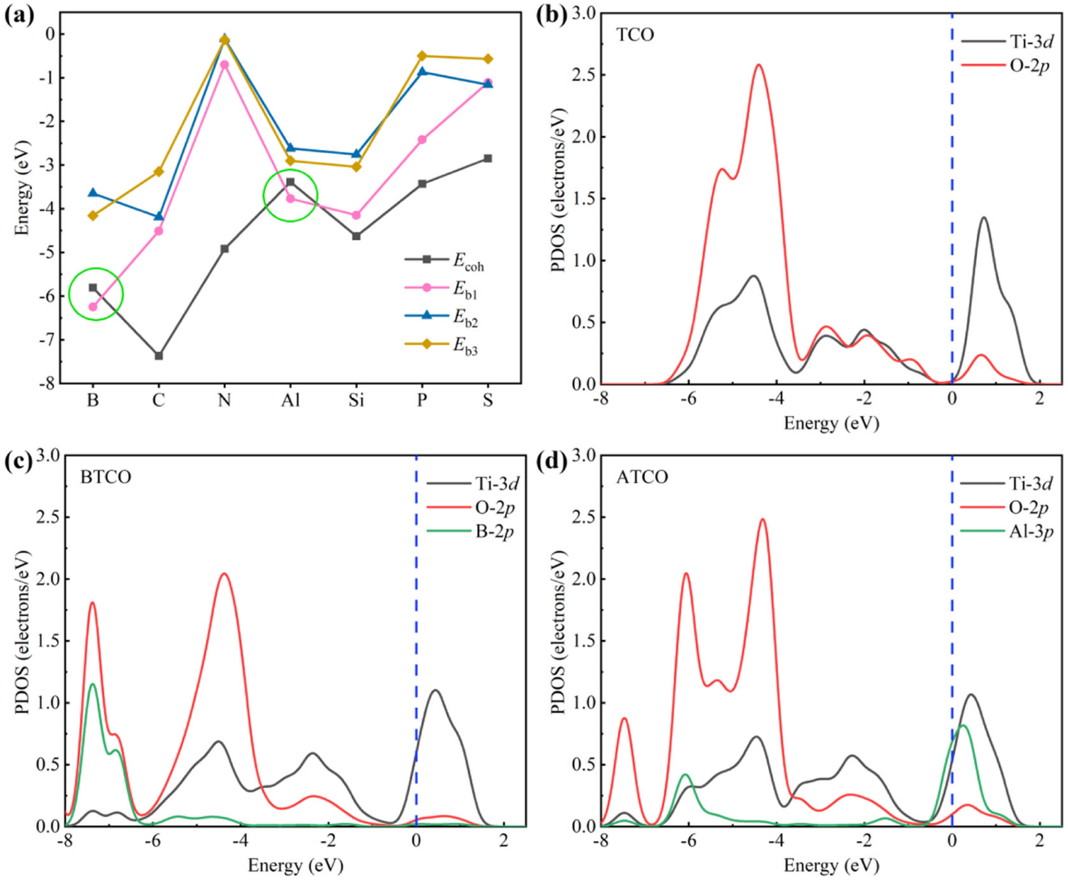

Fig. 2. (a) Comparison between the binding energy of doped elements in Ti_2CO_2 (E_{b1}), Zr_2CO_2 (E_{b2}), Hf_2CO_2 (E_{b3}) and the cohesive energy of the corresponding elements (E_{coh}); The PDOS of TCO (b), BTCO (c) and ATCO (d), the Fermi level is set to zero and marked with dashed line in this and the following figures.

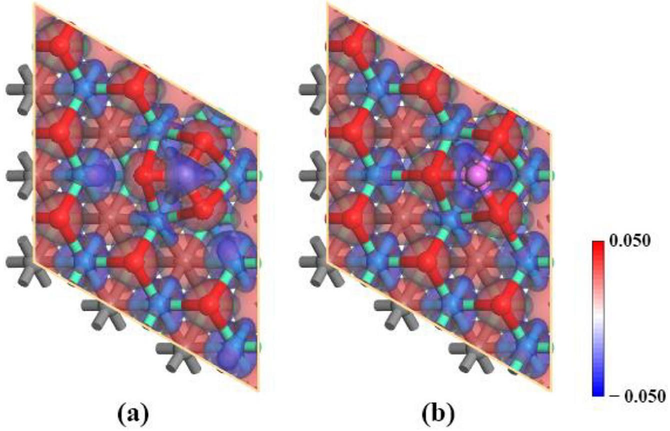

Fig. 3. The DCD of BTCO (a) and ATCO (b). The red and blue areas in this and the following figures represent electron gain and loss, respectively.

K, 500 K and 700 K. In other words, ATCO can exist in a stable way at room temperature and relatively high temperature. Furthermore, a second Al atom is added above the first anchored Al on ATCO monolayer to examine the stability of ATCO. The calculated result shows that the binding energy of the second Al is −2.11 eV, which is lower than that of the first Al atom and the cohesive energy of Al. As Fig. 4(d) depicts, the distance of these two Al atoms is 2.797 Å, so that it's too long for them to form chemical bond. Hence, single Al atom is well dispersed on TCO in the form of SACs.

3.2. ITGs adsorption on TCO and ATCO

The ITGs (CO, NO, NH_3, NO_2, SO_2 and H_2S) are originally placed above the MXenes at about 2.5 Å, so that the adsorption behavior of ITGs can be imitated. After considering all possible adsorption configurations of ITGs molecules, the most stable configurations of these molecules adsorbed on TCO and ATCO surface are investigated.

3.2.1. ITGs adsorption on TCO

First of all, several possible sites are taken into consideration for the ITGs molecules adsorption on the TCO substrate, including the top site right above C, O or Ti atom and the bridge site between Ti and O atom. After calculation, the adsorption energies of ITGs on TCO substrate (E_{ad}), charge transfers of ITGs (Q_I), the distance between ITGs and TCO surface (d) along with the bond lengths of pristine ITGs (l_1) and those of ITGs adsorbed on TCO (l_2) are summarized in Table 1. Table 1 shows that the E_{ad} are from −0.06 to −0.43 eV, the Q_I vary from −0.003 to 0.239 e, and there is barely change in the bond lengths of ITGs before and after adsorbing on TCO. On the basis of Fig. S1, we can see that ITGs have a weak interaction with TCO since there are not obvious change in the structure of ITGs and TCO and chemical bonds are not formed, except for NH_3 [34,45]. In the case of NH_3, we can find that the adsorption energy of NH_3 (−0.43 eV) is more negative than other ITGs, while the distance between NH_3 and TCO surface (1.780 Å) is closer than that of other ITGs. Additionally, the Ti atom over against N atom on the TCO surface has a slightly upward movement, and this phenomenon is not observed in else ITGs. In spite of this, considering of Guo et al.'s opinion, the adsorption energy should be more negative than −0.50 eV to substantially seize gas molecule on solid surface [5]. Therefore, we can draw a conclusion that TCO is not an ideal adsorbent for ITGs.

3.2.2. ITGs adsorption on ATCO

Next, we also calculate adsorption energies (E_{ad}), charge transfers of ITGs, Al atom (Q_I, Q_{Al}) and the bond lengths of ITGs adsorbed on ATCO (l_3) to evaluate adsorption capacity of ATCO. For the ITGs molecules adsorption on ATCO, all potential sites are taken into account and marked in Fig. 4(e). As Table 1 lists, the adsorption energies of ITGs on ATCO are much more negative than that of TCO. In the light of Mulliken charge analysis, Al dopant plays the part of electrons donator in the ATCO system, making it possible for CO, NO, NO_2 and SO_2 to obtain more electrons from ATCO than TCO while NH_3 and H_2S lose less electrons, too. At the same time, the bond lengths of ITGs were elongated in varying degrees after adsorbed on ATCO apart from H_2S. As shown in Fig. 5(a-c), CO, NO and NH_3 possess a semblable connection with ATCO, combining with Al atom by their C or N atom, respectively. What's more, CO and

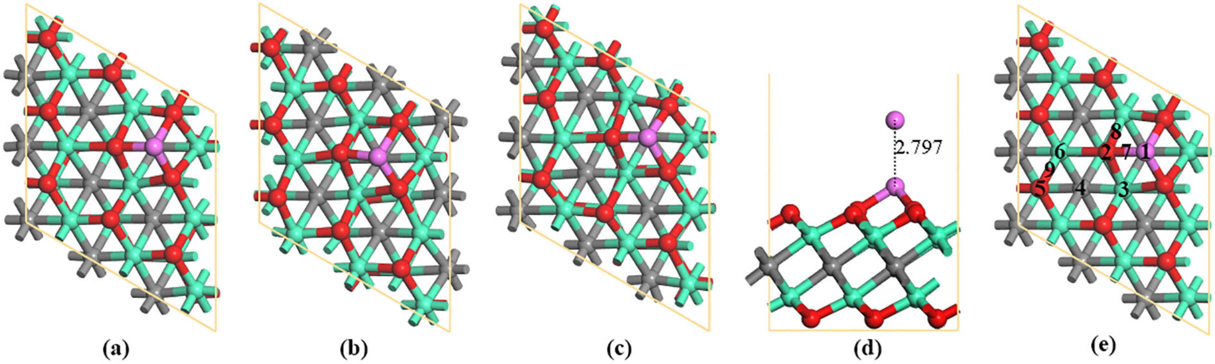

Fig. 4. (a–c) Equilibrated structure of ATCO at the temperature of 300 K (a), 500 K (b) and 700 K (c); (d) Side view of the optimized structure of the second Al atom adsorbed on the ATCO monolayer. (e) The potential adsorption sites including six top sites (1–6) and three bridge sites (7–9) of ATCO.

Table 1

Calculated adsorption energies (E_{ad}), charge transfers of ITGs (Q_I) and Al atom (Q_{Al}), the distance between ITGs and TCO surface (d) and the bond lengths of pristine ITGs (l_1) and those adsorbed on TCO (l_2) and ATCO (l_3). The boldfaces represent the average bond length.

Types	TCO					ATCO			
	E_{ad} (eV)	Q_I (e)	d (Å)	l_1 (Å)	l_2 (Å)	E_{ad} (eV)	Q_I (e)	Q_{Al} (e)	l_3 (Å)
CO	−0.12	0.016	2.749	1.145	1.145	−1.12	−0.108	1.474	1.156
NO	−0.17	0.245	2.374	1.167	1.143	−1.47	−0.306	1.517	1.210
NH_3	−0.43	0.173	1.780	1.023	1.022	−2.24	0.136	1.501	1.030
NO_2	−0.06	0.000	2.378	1.213	1.215	−3.61	−0.513	1.616	**1.285**
SO_2	−0.21	−0.003	2.839	1.464	1.465	−2.45	−0.589	1.612	**1.585**
H_2S	−0.20	0.082	2.346	1.351	1.354	−2.52	0.023	1.279	1.354

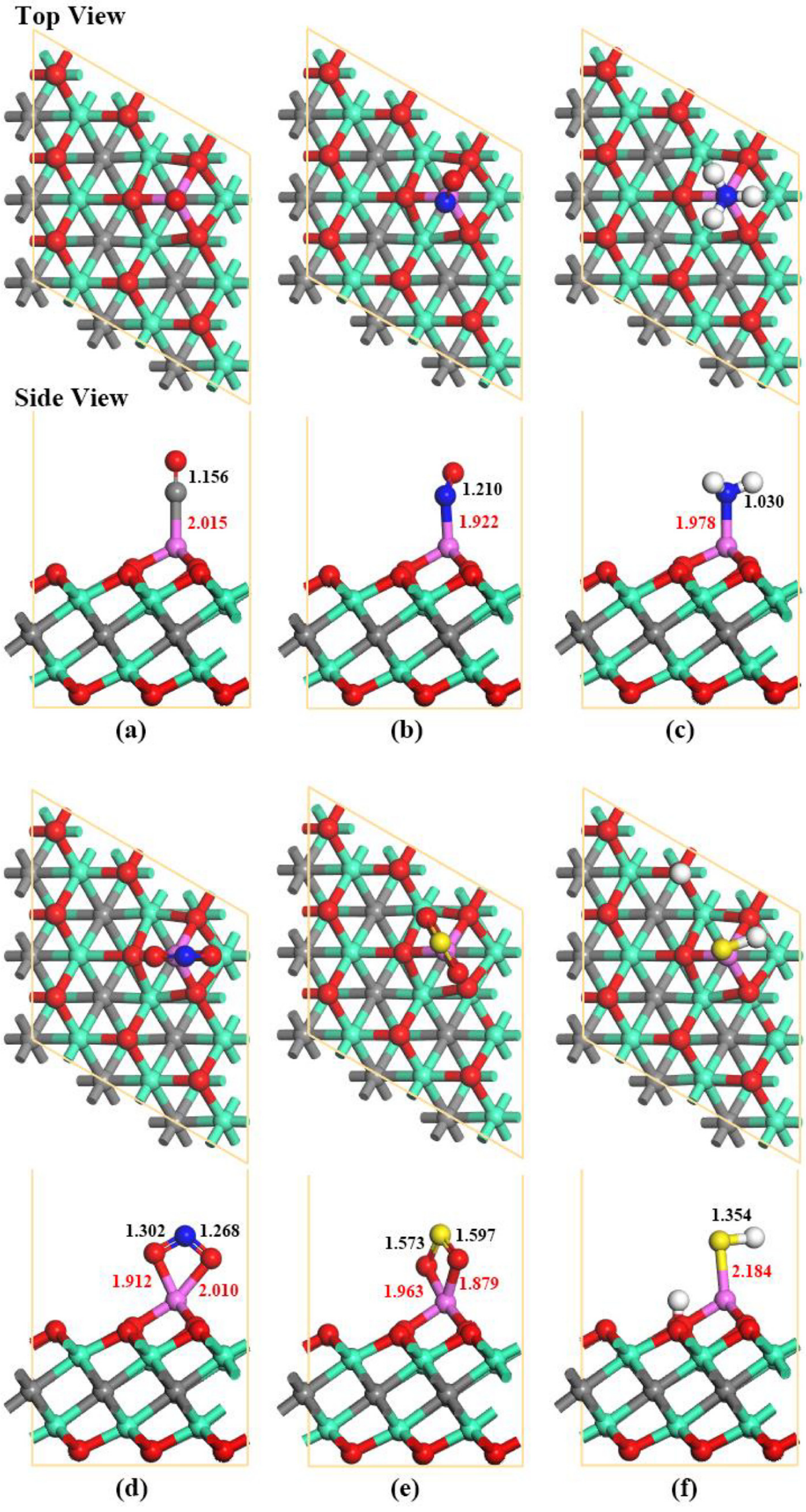

Fig. 5. The most stable configuration of CO (a), NO (b), NH_3 (c), NO_2 (d), SO_2 (e) and H_2S (f) adsorbed on ATCO monolayer. The white, blue and yellow balls in this and the following figures are H, N and S atoms, respectively.

NH_3 tend to be vertically chemisorbed to the Al atom, while NO prefers to be bonded with Al atom with a slightly tilted angle. The bond length of C–Al in CO and N–Al in NO and NH_3 are 2.015 Å, 1.922 Å and 1.978 Å respectively, which is close to the sum of relevant covalent radii of C–Al (2.01 Å) and N–Al (1.97 Å) [64]. As shown in Fig. 5(d) and (e), the Al atom is able to bond with both two O atom in NO_2 and SO_2 and then establish a stable structure. It is worth mentioning that the adsorption energy of NO_2 on ATCO is −3.61 eV, which has tremendous improvement compared to that of NO_2 on TCO. The distances of two O–Al bonds of NO_2 on ATCO are 1.912 Å and 2.010 Å, while those of SO_2 on ATCO are 1.879 Å and 1.963 Å. They are also close to the sum of covalent radii of O and Al (1.89 Å) [64]. In Fig. 5f, for H_2S, one of the H–S bonds are broken, then the H atom from the broken H–S bond is attracted to the O atom on ATCO surface, which is similar to the structure of H_2S adsorption on V-decorated Ti_2CO_2 mentioned above [58]. It means that the first step of H_2S dissociation ($H_2S \rightarrow HS^* + H^*$) can react spontaneously without energy barrier, which is in favor of the subsequent reactions. The S atom is bonded to Al atom with a 2.184 Å bond length, which is shorter than the sum of their covalent radii (2.29 Å) [64]. In general, the ITGs can be chemisorbed on ATCO due to the fact that the distances of their bond lengths with Al atom are lower or close to the corresponding covalent radii.

To further analyze the mechanism in electronic level, the PDOS and DCD are calculated. As Fig. 6 depicts, there is a comparatively large hybridization around the Fermi level of PDOS between CO, NO, NO_2 and SO_2 and Al dopant. Actually, the state density peaks of them at about −8 eV and near the Fermi level are mostly contributed by the *p* orbital of C/N/S and O atom. On the contrary, in the case of NH_3 and H_2S, their PDOS mainly consists of N-2*p* and S-3*p* orbital respectively, lacking of the hybridization of diverse atoms. As shown in Fig. 7, the electron

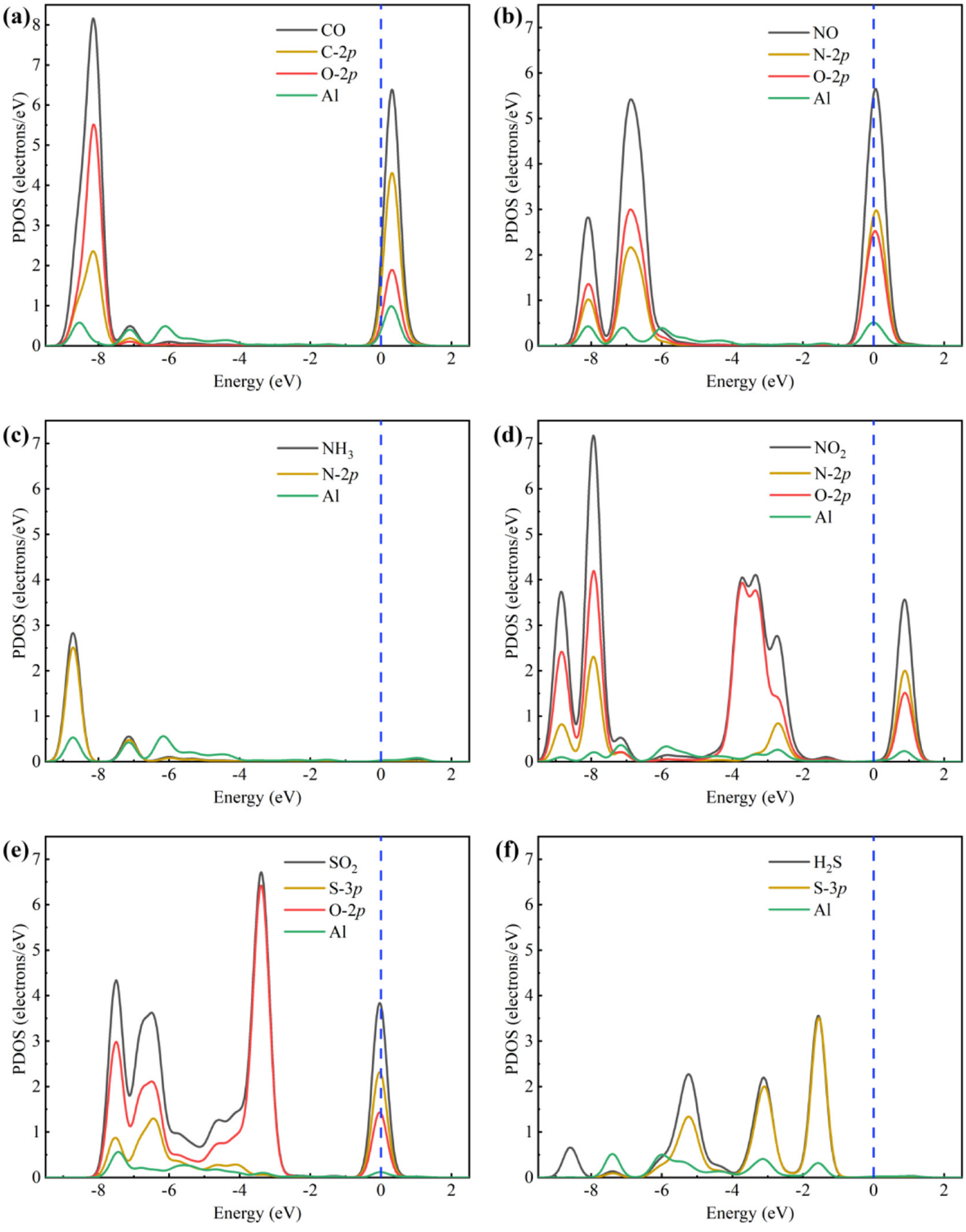

Fig. 6. The PDOS of CO (a), NO (b), NH_3 (c), NO_2 (d), SO_2 (e) and H_2S (f) adsorbed on ATCO monolayer.

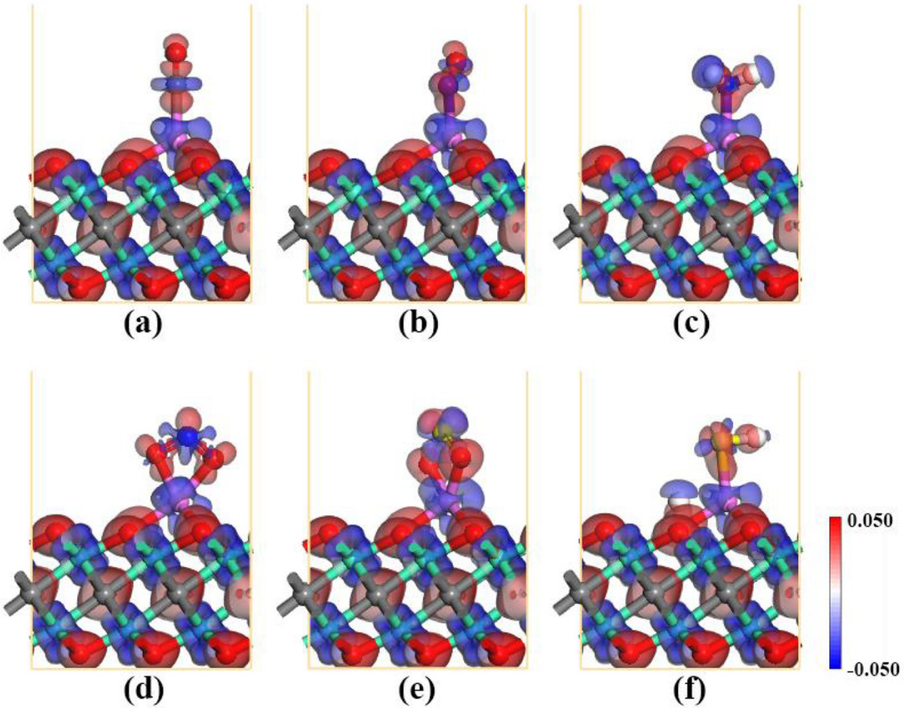

Fig. 7. The DCD on ATCO monolayer with CO (a), NO (b), NH_3 (c), NO_2 (d), SO_2 (e) and H_2S (f).

cloud density emerges and overlaps over a wide range in the vicinity of Al atom and adsorbed ITGs molecules. It can be observed that the Al atoms are surrounded by blue area and the bonds of ITGs connected to Al atoms as well as the O terminations of ATCO are in red area in the DCD, demonstrating that not only the Al atoms lose electrons but also the ITGs molecules and the surface of ATCO obtain electrons. The results clearly manifest that the Al dopant can significantly enhance the adsorption of ITGs and act as bridge to combine ITGs with ATCO substrate in the meanwhile.

3.3. VOCs adsorption on TCO and ATCO

Considering the detection of ITGs on MXenes has been explored in reported researches [65], but the VOCs adsorption on them hasn't been systematically studied, the adsorption capacity of VOCs on TCO and ATCO is evaluated in this section. It is well-known that there are various sorts of VOCs. Particularly, oxygenated volatile organic compounds (OVOCs, including RCHO, RCOOH, RCOOR, RCOR, ROH and ROR, *etc.*) have been diffusely studied in the past decades [6,13,66]. In order to explore the adsorption behavior of some representative VOCs on TCO and ATCO, the adsorption process of three typical kinds of VOCs molecules including OVOCs, aromatic compounds (ACs) and hydrocarbons (HCs) are investigated. The possible sites of VOCs adsorbed on TCO and ATCO surface are identical to those of ITGs.

3.3.1. Adsorption of different VOCs on TCO

The calculated results for these representative VOCs adsorbed on TCO are exhibited in Table 2. As listed in Table 1 and Table 2, we can

Table 2
Calculated adsorption energies (E_{ad}), charge transfers of VOCs (Q_V) and Al atom (Q_{Al}), the $C_1 = O_1/C_1\text{-}O_1$ bond lengths of pristine VOCs (l_1) and those adsorbed on TCO (l_2) and ATCO (l_3) of some common VOCs. The boldfaces represent the average bond length.

Types		TCO				ATCO			
		E_{ad} (eV)	Q_V (e)	l_1 (Å)	l_2 (Å)	E_{ad} (eV)	Q_V (e)	Q_{Al} (e)	l_3 (Å)
RCHO	HCHO	−0.18	0.058	1.217	1.217	−2.13	−0.195	1.648	1.294
	CH_3CHO	−0.28	0.090	1.221	1.222	−2.33	−0.085	1.634	1.292
RCOOH	HCOOH	−0.34	0.038	1.214	1.221	−2.80	−0.265	1.665	1.345
	CH_3COOH	−0.34	0.040	1.220	1.222	−3.27	−0.207	1.658	**1.291**
RCOOR	$HCOOCH_3$	−0.32	0.043	1.216	1.217	−2.20	0.096	1.581	1.269
	$CH_3COOC_2H_5$	−0.48	0.071	1.221	1.224	−2.52	0.162	1.596	1.289
RCOR	CH_3COCH_3	−0.40	0.110	1.228	1.228	−2.47	−0.005	1.625	1.294
	$CH_3COC_2H_5$	−0.43	0.132	1.228	1.229	−2.60	0.019	1.607	1.292
ROH	CH_3OH	−0.33	0.118	1.434	1.434	−2.76	−0.207	1.619	1.431
	C_2H_5OH	−0.35	0.103	1.437	1.443	−2.14	0.152	1.546	1.529
ROR	CH_3OCH_3	−0.41	0.108	1.422	1.429	−2.11	0.139	1.549	1.480
	$C_2H_5OC_2H_5$	−0.43	0.118	1.431	**1.435**	−2.50	0.149	1.557	**1.496**
ACs	C_6H_6	−0.50	0.091	/	/	−1.62	0.207	1.365	/
	C_7H_8	−0.60	0.117	/	/	−1.81	0.233	1.364	/
	C_6H_5OH	−0.64	0.185	/	/	−2.13	0.215	1.399	/
HCs	CH_4	−0.14	0.016	/	/	−0.47	0.118	1.391	/
	C_2H_4	−0.18	0.029	/	/	−1.32	−0.035	1.400	/
	C_2H_2	−0.17	0.036	/	/	−1.25	−0.174	1.492	/

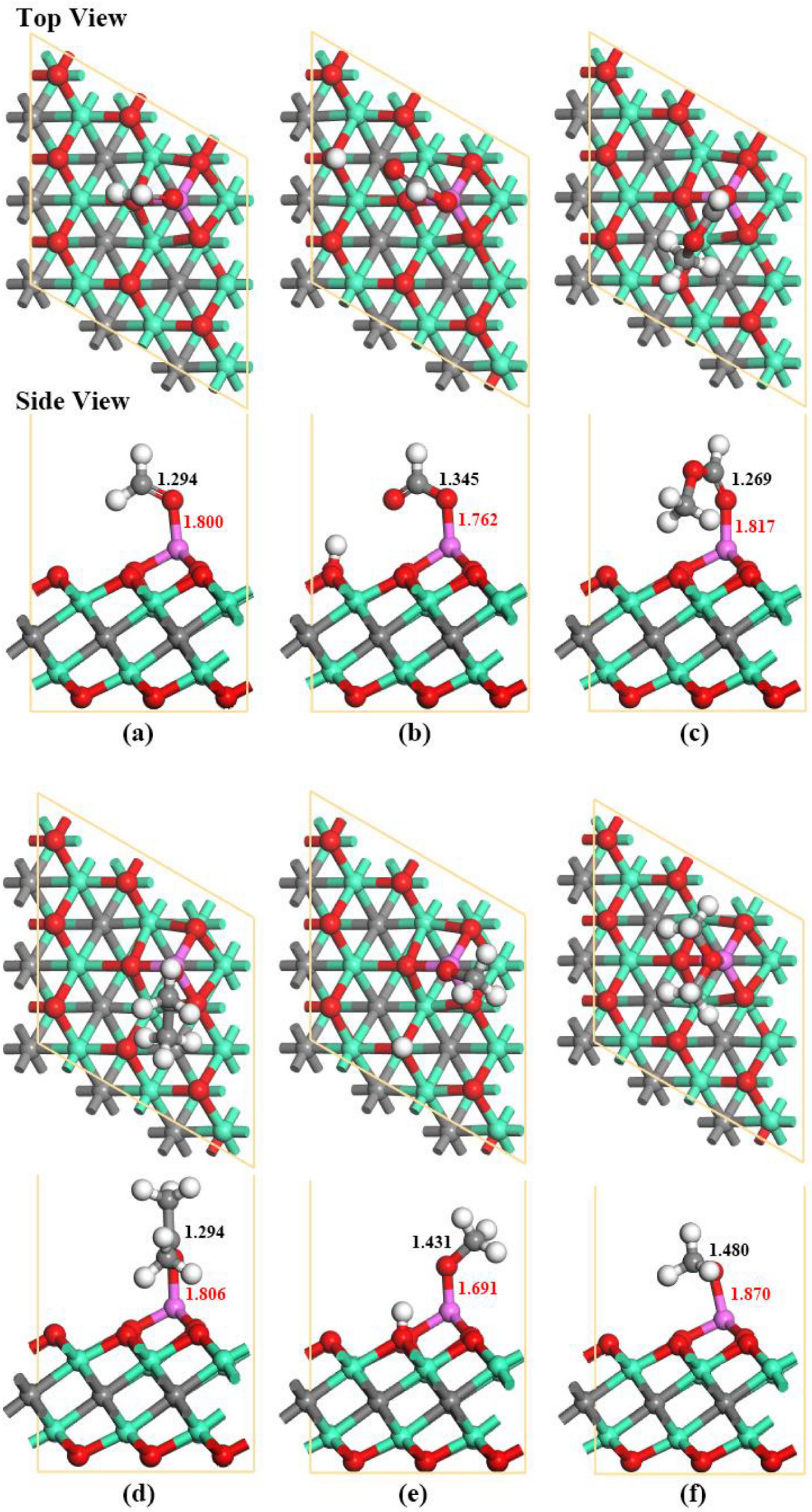

Fig. 8. The most stable configuration of HCHO (a), HCOOH (b), $HCOOCH_3$ (c), CH_3COCH_3 (d), CH_3OH (e) and CH_3OCH_3 (f) adsorbed on ATCO monolayer.

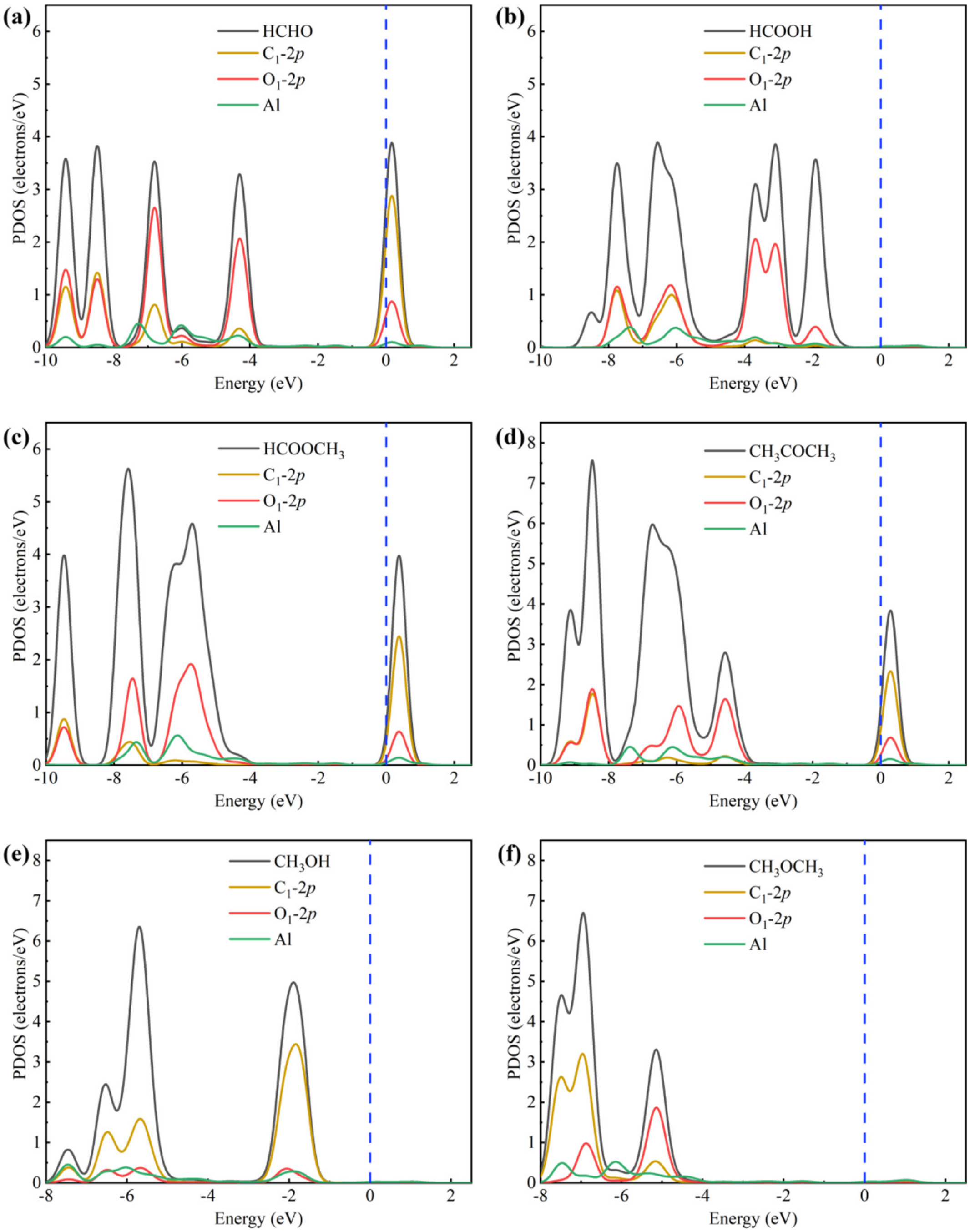

Fig. 9. The PDOS of HCHO (a), HCOOH (b), $HCOOCH_3$ (c), CH_3COCH_3 (d), CH_3OH (e) and CH_3OCH_3 (f) adsorbed on ATCO monolayer.

see that the adsorption energies of OVOCs and ACs on TCO are a little more negative than that of ITGs. But as shown in Fig. S2-S4, VOCs are still not able to have chemisorption on TCO. Interestingly, in the most stable adsorption configurations of OVOCs on TCO monolayer, the O atoms of almost all OVOCs are engaged by the Ti atom on TCO surface, illustrating that there is subsistent interaction between O and Ti atoms.

3.3.2. Adsorption of different VOCs on ATCO

Subsquently, the adsorption of various VOCs molecules on ATCO is further investigated. The corresponding adsorption energies (E_{ad}), Mulliken charge analysis of VOCs and Al atom (Q_V, Q_{Al}) are provided in Table 2. From the table, it is known that the adsorption energies of VOCs on ATCO are stronger than those on TCO, and the adsorption energies of OVOCs on ATCO are normally more negative than those of ACs and HCs at the same time. This suggests that OVOCs reveal more powerful adsorption with ATCO than ACs and HCs, which matches the geometry optimization results. Just as Fig. S2 shows, for benzene, toluene and phenol, they are attracted to ATCO substrate with an inclined angle, but benzene and toluene cannot form a chemical bond with Al atom.

As mentioned above, Al-doped porous graphene has been revealed huge promotion in the adsorption of OVOCs, especially in carbonyl-containing volatile organic compounds (CVOCs) [6], and ATCO is attested to have similar property as well. Fig. 8 and Fig. S5 show the most stable adsorption configuration of some OVOCs on ATCO, all of these OVOCs are connected with ATCO by their O atom. For simplicity, the O atoms in OVOCs that bond with Al atom are identified as O_1, and the C atoms bond with O_1 are defined as C_1 in the following part. In the case of CH_3OH, HCOOH and CH_3COOH, the H–O bond of hydroxyl

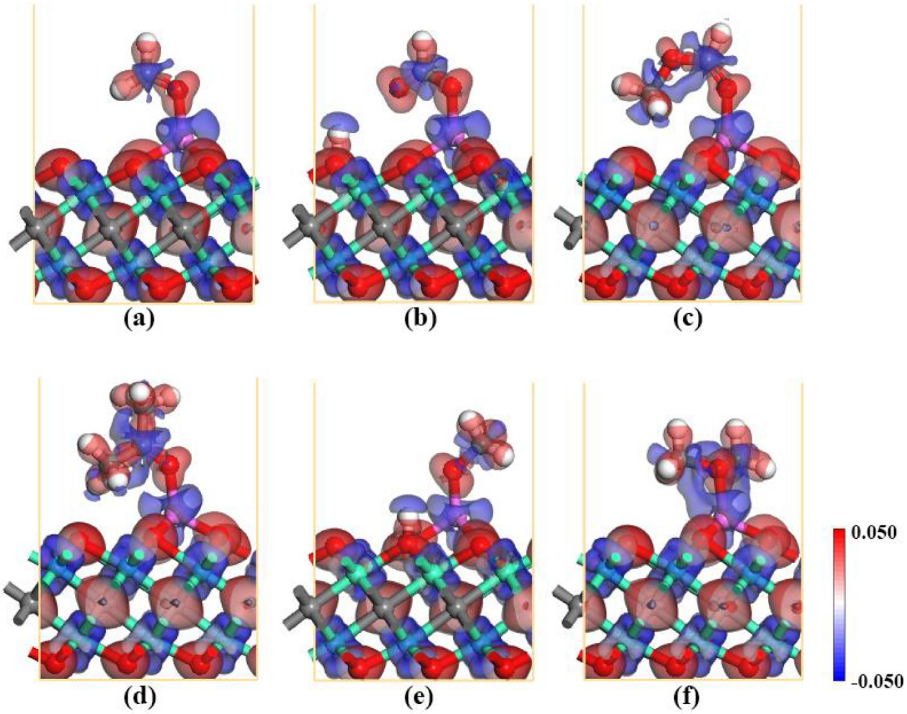

Fig. 10. The DCD on ATCO monolayer with HCHO (a), HCOOH (b), $HCOOCH_3$ (c), CH_3COCH_3 (d), CH_3OH (e) and CH_3OCH_3 (f).

are broken, and the $H_{H\text{-}O}$ atom forms a chemical bond with the O atom on the ATCO surface. After that, for CH_3COOH, the $O_{H\text{-}O}$ atom forms a double bond with the $C_{C=O}$ atom of carbonyl, and this O atom also forms chemical bond with the Al atom. Then, the $O_{C=O}$ atom of carbonyl is bonded to the Al atom with the double C=O bond broken into single bond. Unsurprisingly, similar reaction is happened in HCOOH—the homologue of CH_3COOH, but the $O_{H\text{-}O}$ atom of HCOOH is not attached to Al atom. For the rest of OVOCs (RCHO, RCOOR, RCOR, ROR and C_2H_5OH), they connect to Al atom by their O_1 atom with the $C_1 = O_1$/C_1–O_1 bond undamaged. Most of the O_1–Al bonds are shorter than the sum of their covalent radii (1.89 Å) [64], suggesting that OVOCs are chemisorbed with ATCO monolayer. In short, O atom of OVOCs can attract the Al atom to form an O–Al bond, contributing to the connection of OVOCs and ATCO substrate. On top of this, Table 2 indicates that the bond lengths of $C_1 = O_1$/C_1–O_1 were elongated on a large scale after adsorbed on ATCO except CH_3OH.

To understand the charge transfer between OVOCs and ATCO, Mulliken charge distribution is calculated and exhibited in Table 2. It elaborates that only a small number of charges transfer from the OVOCs molecule to the TCO monolayer. Yet, the OVOCs molecule acquires electrons from the Al atoms, leading to the bigger change of absolute charge on ATCO system. What's more, the PDOS of OVOCs are investigated as reported in Fig. 9 and Fig. S6. These OVOCs both possess various state density peaks below the Fermi level. For RCHO, RCOOR and RCOR, a state density peak around the Fermi level is existed, corresponding to the intact C=O bond of carbonyl due to the fact that the 2*p* orbitals of C_1 and O_1 have a determining impact on the peak near the Fermi level. But for RCOOH, ROH and ROR, their PDOS near the Fermi level are practically zero. On top of this, the DCD of OVOCs is also displayed in Fig. 10 and Fig. S7. Obviously, there is a certain degree of overlap in electron cloud density for all of these adsorbed OVOCs and Al atoms. We can also observe that the Al atoms serve as electrons donators while the O_1 atoms act as receptors. As a result, the positively charged Al atoms can connected with the negatively charged O_1 atoms, promoting the combination of OVOCs and ATCO. In conclusion, we deduce that the Al atom plays a part as a medium to contact the electron clouds of OVOCs and ATCO substrate, which enhances the OVOCs adsorption capacity of ATCO.

In addition, adsorption energies of some gaseous pollutants on other 2D materials and ATCO are illustrated in Table S5. According to this table, the adsorption energies of some ITGs and VOCs on ATCO are much higher than reported results on MXenes and graphene, confirming that ATCO is an outstanding material for the adsorption of gaseous pollutants.

4. Conclusion

In this work, by using DFT calculation, the stability of a series of single-atom-decorated MXenes (A/M_2CO_2, A = B, C, N, Al, Si, P and S, M = Ti, Zr and Hf) are investigated in detail. Among these MXenes, BTCO and ATCO are attested to steadily exist without the formation of aggregated cluster, and ATCO demonstrates more excellent electronic properties than BTCO. Subsequently, ITGs and VOCs adsorption on TCO and ATCO monolayer is systematically studied. Although TCO substrate is proved to be unsuitable as a gas adsorbent, its adsorption energies of ITGs and VOCs (especially in OVOCs) can be greatly improved after doping Al atom. Meanwhile, the mechanism of enhanced adsorption for ATCO is revealed by means of electronic structure analysis including Mulliken charge analysis, PDOS and DCD. We speculate that the decoration of Al atom creates more negative electronic surroundings around the Al atom and facilitates the electron flow to adsorbed gases. Our work provides a potential single-atom-decorated adsorbent ATCO of ITGs and VOCs without noble metals and expands the application of MXenes in the range of environment pollution control.

Declaration of Competing Interest

The authors declare the following financial interests/personal relationships which may be considered as potential competing interests:

Zhimin Ao reports financial support was provided by National Natural Science Foundation of China. Didi Li reports financial support was

provided by National Natural Science Foundation of China. Zhimin Ao reports financial support was provided by Science and Technology Planning Project of Guangdong Province. Didi Li reports financial support was provided by Natural Science Foundation of Guangdong Province. Taicheng An reports financial support was provided by Local Innovative and Research Teams Project of Guangdong Pearl River Talents Program. Taicheng An reports financial support was provided by the Innovation Team Project of Guangdong Provincial Department of Education.

Acknowledgements

This work was supported by National Natural Science Foundation of China (21777033 and 41807191), Science and Technology Planning Project of Guangdong Province (2017B020216003), Natural Science Foundation of Guangdong Province (2018A030310524), Local Innovative and Research Teams Project of Guangdong Pearl River Talents Program (2017BT01Z032), and the Innovation Team Project of Guangdong Provincial Department of Education (2017KCXTD012).

Appendix A. Supplementary data

Supplementary data to this article can be found online at https://doi.org/10.1016/j.susmat.2021.e00294.

References

[1] R. Suarez-Bertoa, A.A. Zardini, S.M. Platt, S. Hellebust, S.M. Pieber, I. El Haddad, B. Temime-Roussel, U. Baltensperger, N. Marchand, A.S.H. Prévôt, C. Astorga, Primary emissions and secondary organic aerosol formation from the exhaust of a flex-fuel (ethanol) vehicle, Atmos. Environ. 117 (2015) 200–211, https://doi.org/10.1016/j.atmosenv.2015.07.006.

[2] W. Yang, H. Chen, J. Wu, W. Wang, J. Zheng, D. Chen, J. Li, X. Tang, Z. Wang, L. Zhu, W. Wang, Characteristics of the source apportionment of primary and secondary inorganic PM2.5 in the Pearl River Delta region during 2015 by numerical modeling, Environ. Pollut. 267 (2020) 115418, https://doi.org/10.1016/j.envpol.2020.115418.

[3] T. Hussain, T. Kaewmaraya, S. Chakraborty, R. Ahuja, Defect and substitution-induced silicene sensor to probe toxic gases, J. Phys. Chem. C 120 (2016) 25256–25262, https://doi.org/10.1021/acs.jpcc.6b08973.

[4] H. Dai, S. Jing, H. Wang, Y. Ma, L. Li, W. Song, H. Kan, VOC characteristics and inhalation health risks in newly renovated residences in Shanghai, China, Sci. Total Environ. 577 (2017) 73–83, https://doi.org/10.1016/j.scitotenv.2016.10.071.

[5] H. Guo, W. Zhang, N. Lu, Z. Zhuo, X.C. Zeng, X. Wu, J. Yang, CO_2 capture on h-BN sheet with high selectivity controlled by external electric field, J. Phys. Chem. C 119 (2015) 6912–6917, https://doi.org/10.1021/acs.jpcc.5b00681.

[6] B. Liu, W. Zhao, Q. Jiang, Z. Ao, T. An, Enhanced adsorption mechanism of carbonyl-containing volatile organic compounds on Al-decorated porous graphene monolayer: a density functional theory calculation study, SM&T 21 (2019), e00103, https://doi.org/10.1016/j.susmat.2019.e00103.

[7] X. Zhang, J. Lei, D. Wu, X. Zhao, Y. Jing, Z. Zhou, A Ti-anchored Ti_2CO_2 monolayer (MXene) as a single-atom catalyst for CO oxidation, J. Mater. Chem. A 4 (2016) 4871–4876, https://doi.org/10.1039/c6ta00554c.

[8] C. He, J. Cheng, X. Zhang, M. Douthwaite, S. Pattisson, Z. Hao, Recent advances in the catalytic oxidation of volatile organic compounds: a review based on pollutant sorts and sources, Chem. Rev. 119 (2019) 4471–4568, https://doi.org/10.1021/acs.chemrev.8b00408.

[9] B. Jing, Z. Ao, Z. Teng, C. Wang, J. Yi, T. An, Density functional theory study on the effects of oxygen groups on band gap tuning of graphitic carbon nitrides for possible photocatalytic applications, SM&T 16 (2018) 12–22, https://doi.org/10.1016/j.susmat.2018.04.001.

[10] B. Jing, Z. Ao, W. Zhao, Y. Xu, Z. Chen, T. An, Evaluation procedure of photocatalysts for VOCs degradation from the view of density functional theory calculations: g-C_3N_4 dots/graphene as an example, J. Mater. Chem. A 8 (2020) 20363–20372, https://doi.org/10.1039/d0ta06060g.

[11] S. Zhang, J. You, C. Kennes, Z. Cheng, J. Ye, D. Chen, J. Chen, L. Wang, Current advances of VOCs degradation by bioelectrochemical systems: a review, Chem. Eng. J. 334 (2018) 2625–2637, https://doi.org/10.1016/j.cej.2017.11.014.

[12] Y. Su, Z. Ao, Y. Ji, G. Li, T. An, Adsorption mechanisms of different volatile organic compounds onto pristine C_2N and Al-doped C_2N monolayer: a DFT investigation, Appl. Surf. Sci. 450 (2018) 484–491, https://doi.org/10.1016/j.apsusc.2018.04.157.

[13] M. Wen, G. Li, H. Liu, J. Chen, T. An, H. Yamashita, Metal–organic framework-based nanomaterials for adsorption and photocatalytic degradation of gaseous pollutants: recent progress and challenges, Environ. Sci. Nano 6 (2019) 1006–1025, https://doi.org/10.1039/c8en01167b.

[14] M. Naguib, M. Kurtoglu, V. Presser, J. Lu, J. Niu, M. Heon, L. Hultman, Y. Gogotsi, M.W. Barsoum, Two-dimensional nanocrystals produced by exfoliation of Ti_3AlC_2, Adv. Mater. 23 (2011) 4248–4253, https://doi.org/10.1002/adma.201102306.

[15] M. Naguib, J. Come, B. Dyatkin, V. Presser, P.-L. Taberna, P. Simon, M.W. Barsoum, Y. Gogotsi, MXene: a promising transition metal carbide anode for lithium-ion batteries, Electrochem. Commun. 16 (2012) 61–64, https://doi.org/10.1016/j.elecom.2012.01.002.

[16] M. Naguib, O. Mashtalir, J. Carle, V. Presser, J. Lu, L. Hultman, Y. Gogotsi, M.W. Barsoum, Two-dimensional transition metal carbides, ACS Nano 6 (2012) 1322–1331, https://doi.org/10.1021/nn204153h.

[17] M. Alhabeb, K. Maleski, B. Anasori, P. Lelyukh, L. Clark, S. Sin, Y. Gogotsi, Guidelines for synthesis and processing of two-dimensional titanium carbide ($Ti_3C_2T_x$ MXene), Chem. Mater. 29 (2017) 7633–7644, https://doi.org/10.1021/acs.chemmater.7b02847.

[18] K.D. Fredrickson, B. Anasori, Z.W. Seh, Y. Gogotsi, A. Vojvodic, Effects of applied potential and water intercalation on the surface chemistry of Ti_2C and Mo_2C MXenes, J. Phys. Chem. C 120 (2016) 28432–28440, https://doi.org/10.1021/acs.jpcc.6b09109.

[19] S. Yi, G. Liu, Z. Liu, W. Hu, H. Deng, Theoretical insights into nitrogen fixation on Ti_2C and Ti_2CO_2 in a lithium–nitrogen battery, J. Mater. Chem. A 7 (2019) 19950–19960, https://doi.org/10.1039/c9ta06232g.

[20] P. Srivastava, A. Mishra, H. Mizuseki, K.R. Lee, A.K. Singh, Mechanistic insight into the chemical exfoliation and functionalization of Ti_3C_2 MXene, ACS Appl. Mater. Interfaces 8 (2016) 24256–24264, https://doi.org/10.1021/acsami.6b08413.

[21] Q. Sun, J. Wang, X. Wang, J. Dai, X. Wang, H. Fan, Z. Wang, H. Li, X. Huang, W. Huang, Treatment-dependent surface chemistry and gas sensing behavior of the thinnest member of titanium carbide MXenes, Nanoscale 12 (2020) 16987–16994, https://doi.org/10.1039/c9nr08350b.

[22] Y. Xie, M. Naguib, V.N. Mochalin, M.W. Barsoum, Y. Gogotsi, X. Yu, K.W. Nam, X.Q. Yang, A.I. Kolesnikov, P.R. Kent, Role of surface structure on Li-ion energy storage capacity of two-dimensional transition-metal carbides, J. Am. Chem. Soc. 136 (2014) 6385–6394, https://doi.org/10.1021/ja501520b.

[23] Z. Jin, C. Liu, Z. Liu, J. Han, Y. Fang, Y. Han, Y. Niu, Y. Wu, C. Sun, Y. Xu, Rational design of hydroxyl-rich $Ti_3C_2T_x$ MXene quantum dots for high-performance electrochemical N_2 reduction, Adv. Energy Mater. 10 (2020) 2000797, https://doi.org/10.1002/aenm.202000797.

[24] C.E. Shuck, Y. Gogotsi, Taking MXenes from the lab to commercial products, Chem. Eng. J. 401 (2020) 125786, https://doi.org/10.1016/j.cej.2020.125786.

[25] J. Peng, X. Chen, W.-J. Ong, X. Zhao, N. Li, Surface and heterointerface engineering of 2D MXenes and their nanocomposites: insights into electro- and photocatalysis, Chem 5 (2019) 18–50, https://doi.org/10.1016/j.chempr.2018.08.037.

[26] M. Khazaei, A. Ranjbar, M. Arai, T. Sasaki, S. Yunoki, Electronic properties and applications of MXenes: a theoretical review, J. Mater. Chem. C 5 (2017) 2488–2503, https://doi.org/10.1039/c7tc00140a.

[27] Y. Gogotsi, B. Anasori, The rise of MXenes, ACS Nano 13 (2019) 8491–8494, https://doi.org/10.1021/acsnano.9b06394.

[28] Z. Guo, J. Zhou, L. Zhu, Z. Sun, MXene: a promising photocatalyst for water splitting, J. Mater. Chem. A 4 (2016) 11446–11452, https://doi.org/10.1039/c6ta04414j.

[29] C. Fu, X. Li, Q. Luo, J. Yang, Two-dimensional multilayer M_2CO_2 (M = Sc, Zr, Hf) as photocatalysts for hydrogen production from water splitting: a first principles study, J. Mater. Chem. A 5 (2017) 24972–24980, https://doi.org/10.1039/c7ta08812d.

[30] J. Zhang, Y. Zhao, X. Guo, C. Chen, C.-L. Dong, R.-S. Liu, C.-P. Han, Y. Li, Y. Gogotsi, G. Wang, Single platinum atoms immobilized on an MXene as an efficient catalyst for the hydrogen evolution reaction, Nat. Catal. 1 (2018) 985–992, https://doi.org/10.1038/s41929-018-0195-1.

[31] Y. Chen, W. Gu, L. Tan, Z. Ao, T. An, S. Wang, Photocatalytic H_2O_2 production using Ti_3C_2 MXene as a non-noble metal cocatalyst, Appl. Catal. A Gen. 618 (2021) 118127, https://doi.org/10.1016/j.apcata.2021.118127.

[32] Q. Hu, D. Sun, Q. Wu, H. Wang, L. Wang, B. Liu, A. Zhou, J. He, MXene: a new family of promising hydrogen storage medium, J. Phys. Chem. A 117 (2013) 14253–14260, https://doi.org/10.1021/jp409585v.

[33] B. Anasori, M.R. Lukatskaya, Y. Gogotsi, 2D metal carbides and nitrides (MXenes) for energy storage, Nat. Rev. Mater. 2 (2017) 16098, https://doi.org/10.1038/natrevmats.2016.98.

[34] X. Yu, Y. Li, J. Cheng, Z. Liu, Q.Z. Li, W.Z. Li, X. Yang, B. Xiao, Monolayer Ti_2CO_2: a promising candidate for NH_3 sensor or capturer with high sensitivity and selectivity, ACS Appl. Mater. Interfaces 7 (2015) 13707–13713, https://doi.org/10.1021/acsami.5b03737.

[35] B. Xiao, Y. Li, X. Yu, J. Cheng, MXenes: reusable materials for NH_3 sensor or capturer by controlling the charge injection, Sensors Actuators B Chem. 235 (2016) 103–109, https://doi.org/10.1016/j.snb.2016.05.062.

[36] W. Zhao, N. Yun, Z. Dai, Y. Li, A high-performance trace level acetone sensor using an indispensable $V_4C_3T_x$ MXene, RSC Adv. 10 (2020) 1261–1270, https://doi.org/10.1039/c9ra09069j.

[37] S.N. Shuvo, A.M. Ulloa Gomez, A. Mishra, W.Y. Chen, A.M. Dongare, L.A. Stanciu, Sulfur-doped titanium carbide MXenes for room-temperature gas sensing, ACS Sens. 5 (2020) 2915–2924, https://doi.org/10.1021/acssensors.0c01287.

[38] F. Shahzad, M. Alhabeb, C.B. Hatter, B. Anasori, S.M. Hong, C.M. Koo, Y. Gogotsi, Electromagnetic interference shielding with 2D transition metal carbides (MXenes), Science 353 (2016) 1137–1140, https://doi.org/10.1126/science.aag2421.

[39] M. Khazaei, M. Arai, T. Sasaki, C.-Y. Chung, N.S. Venkataramanan, M. Estili, Y. Sakka, Y. Kawazoe, Novel electronic and magnetic properties of two-dimensional transition metal carbides and nitrides, Adv. Funct. Mater. 23 (2013) 2185–2192, https://doi.org/10.1002/adfm.201202502.

[40] X. Zha, K. Luo, Q. Li, Q. Huang, J. He, X. Wen, S. Du, Role of the surface effect on the structural, electronic and mechanical properties of the carbide MXenes, EPL 111 (2015) 26007, https://doi.org/10.1209/0295-5075/111/26007.

[41] H. Zhang, G. Yang, X. Zuo, H. Tang, Q. Yang, G. Li, Computational studies on the structural, electronic and optical properties of graphene-like MXenes (M_2CT_2, M = Ti, Zr, Hf; T = O, F, OH) and their potential applications as visible-light driven

photocatalysts, J. Mater. Chem. A 4 (2016) 12913–12920, https://doi.org/10.1039/c6ta04628b.

[42] J. Zhou, D. Li, W. Zhao, B. Jing, Z. Ao, T. An, First-principles evaluation of volatile organic compounds degradation in Z-scheme photocatalytic systems: MXene and graphitic-CN heterostructures, ACS Appl. Mater. Interfaces (2021)https://doi.org/10.1021/acsami.1c05617.

[43] K. Xiong, P. Wang, G. Yang, Z. Liu, H. Zhang, S. Jin, X. Xu, Functional group effects on the photoelectronic properties of MXene (Sc_2CT_2, T = O, F, OH) and their possible photocatalytic activities, Sci. Rep. 7 (2017) 15095, https://doi.org/10.1038/s41598-017-15233-8.

[44] Q. Peng, J. Zhou, J. Chen, T. Zhang, Z. Sun, Cu single atoms on Ti_2CO_2 as a highly efficient oxygen reduction catalyst in a proton exchange membrane fuel cell, J. Mater. Chem. A 7 (2019) 26062–26070, https://doi.org/10.1039/c9ta08297b.

[45] A. Junkaew, R. Arroyave, Enhancement of the selectivity of MXenes (M_2C, M = Ti, V, Nb, Mo) via oxygen-functionalization: promising materials for gas-sensing and -separation, Phys. Chem. Chem. Phys. 20 (2018) 6073–6082, https://doi.org/10.1039/c7cp08622a.

[46] Y. Wang, S. Ma, L. Wang, Z. Jiao, A novel highly selective and sensitive NH_3 gas sensor based on monolayer Hf_2CO_2, Appl. Surf. Sci. 492 (2019) 116–124, https://doi.org/10.1016/j.apsusc.2019.06.212.

[47] B. Qiao, A. Wang, X. Yang, L.F. Allard, Z. Jiang, Y. Cui, J. Liu, J. Li, T. Zhang, Single-atom catalysis of CO oxidation using Pt_1/FeO_x, Nat. Chem. 3 (2011) 634–641, https://doi.org/10.1038/nchem.1095.

[48] S. Weon, D. Huang, K. Rigby, C. Chu, X. Wu, J.-H. Kim, Environmental materials beyond and below the nanoscale: single-atom catalysts, ACS ES&T Eng. 1 (2021) 157–172, https://doi.org/10.1021/acsestengg.0c00136.

[49] H. Liu, Z. Hu, Q. Liu, P. Sun, Y. Wang, S. Chou, Z. Hu, Z. Zhang, Single-atom Ru anchored in nitrogen-doped MXene ($Ti_3C_2T_x$) as an efficient catalyst for the hydrogen evolution reaction at all pH values, J. Mater. Chem. A 8 (2020) 24710–24717, https://doi.org/10.1039/d0ta09538a.

[50] C. Cheng, X. Zhang, M. Wang, S. Wang, Z. Yang, Single Pd atomic catalyst on Mo_2CO_2 monolayer (MXene): unusual activity for CO oxidation by trimolecular Eley-Rideal mechanism, Phys. Chem. Chem. Phys. 20 (2018) 3504–3513, https://doi.org/10.1039/c7cp07161b.

[51] X. Yang, Z. Lu, C. Cheng, Y. Wang, X. Zhang, Z. Yang, W. Lu, Identification of efficient single-atom catalysts based on V_2CO_2 MXene by ab initio simulations, J. Phys. Chem. C 124 (2020) 4090–4100, https://doi.org/10.1021/acs.jpcc.9b09912.

[52] Y. Gao, H. Zhuo, Y. Cao, X. Sun, G. Zhuang, S. Deng, X. Zhong, Z. Wei, J. Wang, A theoretical study of electrocatalytic ammonia synthesis on single metal atom/MXene, Chin. J. Catal. 40 (2019) 152–159, https://doi.org/10.1016/s1872-2067(18)63197-3.

[53] B. Huang, N. Li, W.-J. Ong, N. Zhou, Single atom-supported MXene: how single-atomic-site catalysts tune the high activity and selectivity of electrochemical nitrogen fixation, J. Mater. Chem. A 7 (2019) 27620–27631, https://doi.org/10.1039/c9ta09776g.

[54] Y. Su, W. Li, G. Li, Z. Ao, T. An, Density functional theory investigation of the enhanced adsorption mechanism and potential catalytic activity for formaldehyde degradation on Al-decorated C_2N monolayer, Chin. J. Catal. 40 (2019) 664–672, https://doi.org/10.1016/s1872-2067(18)63201-2.

[55] Z.M. Ao, J. Yang, S. Li, Q. Jiang, Enhancement of CO detection in Al doped graphene, Chem. Phys. Lett. 461 (2008) 276–279, https://doi.org/10.1016/j.cplett.2008.07.039.

[56] G. Liu, J. Zhou, W. Zhao, Z. Ao, T. An, Single atom catalytic oxidation mechanism of formaldehyde on Al doped graphene at room temperature, Chin. Chem. Lett. 31 (2020) 1966–1969, https://doi.org/10.1016/j.cclet.2019.12.023.

[57] J. Zhou, G. Liu, Q. Jiang, W. Zhao, Z. Ao, T. An, Density functional theory calculations on single atomic catalysis: Ti-decorated $Ti_3C_2O_2$ monolayer (MXene) for HCHO oxidation, Chin. J. Catal. 41 (2020) 1633–1644, https://doi.org/10.1016/s1872-2067(20)63571-9.

[58] J. Zhou, Z. Ao, T. An, DFT study of the decomposition mechanism of H_2S on V-decorated Ti_2CO_2 single-atom catalyst, Acta Phys. -Chim. Sin. 37 (2021) 2007086, https://doi.org/10.3866/pku.Whxb202007086.

[59] B. Delley, From molecules to solids with the DMol3 approach, J. Chem. Phys. 113 (2000) 7756–7764, https://doi.org/10.1063/1.1316015.

[60] J.P. Perdew, K. Burke, M. Ernzerhof, Generalized gradient approximation made simple, Phys. Rev. Lett. 77 (1996) 3865–3868.

[61] S. Grimme, Semiempirical GGA-type density functional constructed with a long-range dispersion correction, J. Comput. Chem. 27 (2006) 1787–1799, https://doi.org/10.1002/jcc.20495.

[62] B. Delley, Hardness conserving semilocal pseudopotentials, Phys. Rev. B 66 (2002) 155125, https://doi.org/10.1103/PhysRevB.66.155125.

[63] Y. Zhu, S. Murali, W. Cai, X. Li, J.W. Suk, J.R. Potts, R.S. Ruoff, Graphene and graphene oxide: synthesis, properties, and applications, Adv. Mater. 22 (2010) 3906–3924, https://doi.org/10.1002/adma.201001068.

[64] P. Pyykko, M. Atsumi, Molecular single-bond covalent radii for elements 1-118, Chemistry 15 (2009) 186–197, https://doi.org/10.1002/chem.200800987.

[65] Y. Zhang, L. Wang, N. Zhang, Z. Zhou, Adsorptive environmental applications of MXene nanomaterials: a review, RSC Adv. 8 (2018) 19895–19905, https://doi.org/10.1039/c8ra03077d.

[66] M. Yao, Y. Ji, H. Wang, Z. Ao, G. Li, T. An, Adsorption mechanisms of typical carbonyl-containing volatile organic compounds on anatase TiO_2 (001) surface: a DFT investigation, J. Phys. Chem. C 121 (2017) 13717–13722, https://doi.org/10.1021/acs.jpcc.7b02964.